

Nuclear dynamics in the core-excited state of aqueous ammonia probed by resonant inelastic soft x-ray scattering

L. Weinhardt,^{1,*} M. Weigand,^{1,†} O. Fuchs,¹ M. Bär,² M. Blum,^{3,4} J. D. Denlinger,⁴ W. Yang,⁴ E. Umbach,⁵ and C. Heske³

¹Universität Würzburg, Experimentelle Physik VII, Am Hubland, D-97074 Würzburg, Germany

²Helmholtz Zentrum Berlin für Materialien und Energie GmbH, Solar Energy Research, Hahn-Meitner-Platz 1, D-14109 Berlin, Germany.

³Department of Chemistry, University of Nevada, Las Vegas, Nevada 89154-4003, USA

⁴Advanced Light Source, Lawrence Berkeley National Laboratory, 1 Cyclotron Road, Berkeley, California 94720, USA

⁵Karlsruhe Institute of Technology, D-76021 Karlsruhe, Germany

(Received 8 April 2011; revised manuscript received 21 June 2011; published 8 September 2011)

The electronic structure of aqueous NH₃ and ND₃ has been investigated using resonant inelastic soft x-ray scattering. Spectral features of different processes involving nuclear dynamics in the core-excited state can be identified. When exciting into the lowest core-excited state, we find a strong isotope effect and clear evidence for ultrafast proton dynamics. Furthermore, a strong vibronic coupling is observed and, in the case of aqueous NH₃, a vibrational fine structure can be resolved.

DOI: [10.1103/PhysRevB.84.104202](https://doi.org/10.1103/PhysRevB.84.104202)

PACS number(s): 61.25.Em, 33.20.Rm, 78.70.En

I. INTRODUCTION

In recent years, soft x-ray spectroscopies have developed into versatile tools to study the electronic structure of molecular liquids and solutions under ambient conditions. These spectroscopies, in particular, soft x-ray absorption (XAS) and x-ray emission (XES) spectroscopy, have been successfully used to extract information about intermolecular interactions (e.g., hydrogen bonding) in a liquid environment.^{1–4} In the case of water, a vivid discussion about the influence of the hydrogen-bonding environment and ultrafast dynamics in the core-excited state on the XES spectra has occurred,^{5–10} indicating the importance of a detailed understanding of such effects.

Resonant XES (or resonant inelastic soft x-ray scattering, RIXS), as well as resonant Auger (AES) and photoelectron (PES) spectroscopy have also been used as probes to study dynamics in the core-excited state of molecules in the gas phase.^{11–16} Using the core-hole life time as an internal clock, which can be “accelerated” by detuned excitation, it was shown that it is possible to derive information about vibronic coupling^{12,15,16} as well as ultrafast dissociation processes.^{12–14} In the case of liquids, an influence of the (hydrogen-bonding) environment on the vibronic structure as well as on dissociation processes can be expected. For XES of liquid water, the influence of ultrafast dissociation processes is controversially discussed in the literature.^{5–7,17}

In the present work, we study aqueous ammonia solutions (i.e., of NH₃ in H₂O and ND₃ in D₂O) as a model system to investigate the signature of nuclear dynamics, i.e., vibronic coupling and dissociation processes, in N *K* XES and XAS spectra. Furthermore, we employ the RIXS map approach^{10,18} to study and discuss the resonant behavior. As is well known, ammonia, especially in aqueous environment, plays a central role in the nitrogen cycle of biological systems and is of importance for a large number of chemical processes. In the gas phase, ammonia has been investigated by XAS,¹⁹ nonresonant XES,²⁰ and resonant AES.¹¹ In the latter study, evidence for dissociation of the molecule could be found when exciting into the first absorption resonance. In our present work, we will show that similar dissociation processes also take place for

ammonia in the hydrogen-bonding environment of an aqueous solution. Using the N *K* RIXS maps, we find a general signature for such dissociation processes. Furthermore, we find a strong vibronic coupling and observe vibrational progressions for aqueous NH₃.

II. EXPERIMENTAL

Resonant x-ray emission spectra were recorded at Beamline 8.0 of the Advanced Light Source (ALS), Lawrence Berkeley National Laboratory, using a high-transmission soft x-ray spectrometer with an entrance slitless design, a spherical collecting mirror, a variable line spacing grating, and a soft x-ray CCD.²¹ The resolving power $E/\Delta E$ was set to be better than 1000 for both the x-ray spectrometer and the beamline. Excitation and emission energy scales were calibrated using the first vibrational resonance of gas-phase N₂ and the elastically scattered (Rayleigh) line at this energy. The angle between exciting the synchrotron beam and spectrometer was 30° in backscattering geometry. The optical axis of the spectrometer was within the plane defined by the synchrotron beam and its polarization vector. Saturated solutions of NH₃ in H₂O and ND₃ in D₂O, corresponding to concentrations of 18 mol/liter, were investigated at a temperature of 7 °C–8 °C. Note that at this pH (~12.3) only a minor fraction (<0.1%) of the NH₃ (ND₃) is protonated, forming NH₄⁺ (ND₄⁺). The liquid was continuously pumped through our flow-through liquid cell,²² replacing the solution in the probed volume more than ten times per second. Liquid cell and vacuum chamber were separated by a (nitrogen-free) SiC window membrane.

III. RESULTS AND DISCUSSION

The nonresonant N *K* emission spectra of the saturated solutions of NH₃ in H₂O (black, “aqueous NH₃” in the following) and ND₃ in D₂O (red, “aqueous ND₃” in the following) are shown in Fig. 1 ($h\nu_{\text{excitation}} = 409.5$ eV). As expected, the overall spectral shape is quite similar for both solutions, showing emission from the valence orbitals of ammonia, namely with $2a_1^{-1}$, $1e^{-1}$, and $3a_1^{-1}$ valence hole final states (as labeled in Fig. 1). Due to its predominant *s*-type

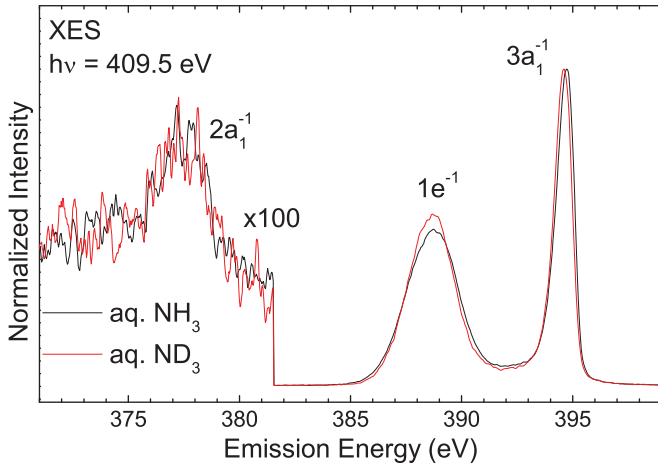


FIG. 1. (Color online) Nonresonant ($h\nu_{\text{excitation}} = 409.5$ eV) N K soft x-ray emission spectra of aqueous NH_3 (black) and aqueous ND_3 (red) solutions, normalized to the peak maximum. Next to each emission feature, the corresponding final state is given. Note that the spectral region of the $2a_1^{-1}$ feature is magnified by a factor of 100.

symmetry, the matrix element for a $2a_1^{-1}$ final state after N $1s$ core excitation is largely dipole forbidden, resulting in a very low intensity of the corresponding emission (magnified by a factor of 100 in Fig. 1). Close inspection of the spectra reveals differences in the energetic position, peak width, and peak shape of the $1e^{-1}$ and $3a_1^{-1}$ emission lines. For aqueous ND_3 , these lines are shifted by ~ 0.1 eV to lower emission energies and have a slightly smaller width ($1e^{-1}$: 2.51 eV; $3a_1^{-1}$: 0.96 eV) than for aqueous NH_3 ($1e^{-1}$: 2.61 eV; $3a_1^{-1}$: 0.99 eV). When normalized to the $3a_1^{-1}$ intensity, the peak area of the $1e^{-1}$ line is slightly larger (by 2%) for ND_3 than for NH_3 . This is likely due to the fact that these peaks consist of (unresolved) vibrational progressions from symmetric bend and stretching modes, as discussed in Ref. 23. Since the vibrational energies of ND_3 are smaller than those of NH_3 (e.g., 300 meV for ND_3 vs 414 meV for NH_3 for the symmetric stretching mode in the electronic ground state in the gas phase²⁴), ND_3 exhibits a narrower progression and slightly different matrix elements than NH_3 .

After discussing the nonresonant spectra, we will now describe the effects of resonant excitation. Usually, a resonant soft x-ray emission experiment consists of a series of spectra at selected excitation energies around the absorption edge. Thanks to the high transmission of our spectrometer, we are able to measure an entire x-ray emission spectrum with good signal-to-noise ratio *at each energy step* in a conventional (narrow-spaced) x-ray absorption scan. The measured data is then best presented in a two-dimensional RIXS map, where the x-ray emission intensity is color coded as a function of excitation (ordinate) and emission (abscissa) energy.^{10,18,21} The N K RIXS maps of aqueous NH_3 and ND_3 are shown in Fig. 2. The RIXS maps can be divided into four regions. First, the observed intensity below an emission energy of ~ 396 eV can be attributed to spectator emission involving the valence hole final states previously discussed (and also labeled in Fig. 2). Second, emission intensity above ~ 397 eV is related to participator emission and dominated by the Rayleigh line (i.e.,

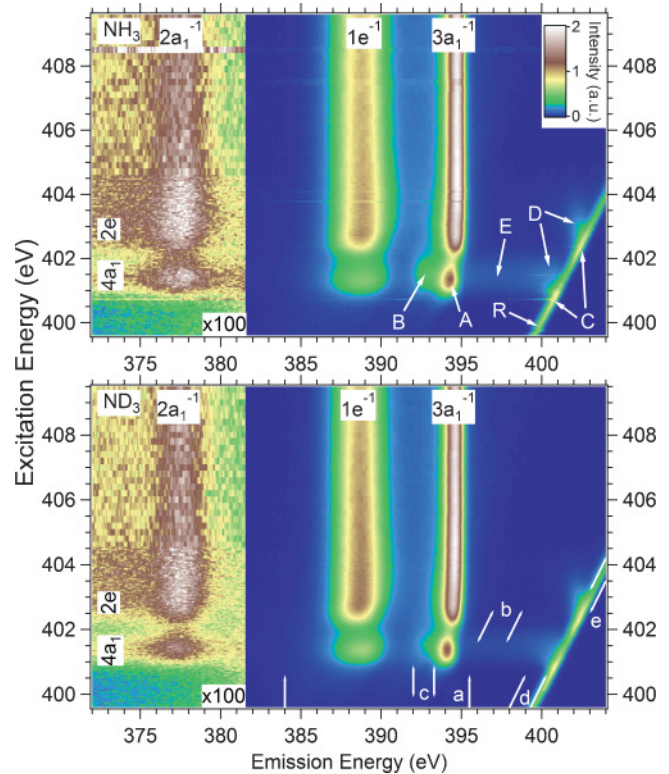


FIG. 2. (Color online) N K RIXS maps of aqueous NH_3 (top) and aqueous ND_3 (bottom). Emission final states and absorption resonances are given on the top and left of each map, respectively. Prominent resonant features are labeled with capital letters in the map of NH_3 . Letters and white lines in the ND_3 map mark the integration regions for the absorption spectra in Fig. 4. Note that the map region of the $2a_1^{-1}$ feature is magnified by a factor of 100.

the elastic line with equal excitation and emission energies). Then, in the excitation energy direction, strong resonant effects can be observed below an excitation energy of ~ 403.5 eV in the region of the $4a_1$ and $2e$ absorption resonances (denoted on the left side of each map), while the region above ~ 403.5 eV is characterized by only weak intensity variations and spectator emission energies that are independent of excitation energy; they appear as vertical lines in the RIXS map.

Besides a strong overall intensity variation as a function of excitation energy, corresponding to the traditional x-ray absorption signal (to be discussed later), several resonant effects can be observed and will be described in the following. With increasing excitation energy between 400 and 402 eV, we observe a shift of the $3a_1^{-1}$ emission towards higher emission energies. Below 401 eV (i.e., just below the $4a_1$ resonance), this shift is “Raman-like”, i.e., it tracks the change in excitation energy (compare with the Rayleigh line, indicated by an “R” in the NH_3 map). Between 401 and 402 eV (region A in the NH_3 map), the shift is a “below-Raman” shift, i.e., the peak shifts less than the Rayleigh line, which can be explained by a coupling to vibrations—depending on the parameters of the potential surfaces of the involved states, such coupling can lead to non-Raman (or even anti-Raman) behavior, as described by Gel’ mukhanov *et al.*²⁵ Furthermore, the $3a_1^{-1}$ emission of both solutions develops a shoulder at lower emission energies (B

in the NH_3 map). This shoulder, as well as features C–E, is further discussed in conjunction with Fig. 3 in the following.

Figure 3(a) compares the XES spectra of aqueous NH_3 with nonresonant excitation (409.5 eV, blue) and excitation into the $4a_1$ absorption resonance (401.3 eV, black), while Fig. 3(b) shows the resonantly excited spectra (401.3 eV) for aqueous NH_3 (black) and aqueous ND_3 (red). The emission corresponding to regions A and B is labeled in Fig. 3(a) as well. We find that the previously mentioned shoulder in region B is also present for aqueous ND_3 , but with lower intensity. The presence of the shoulder and the significant isotope effect cannot solely be explained on the basis of (differences in) the vibrational progressions of aqueous NH_3 and ND_3 —one would expect these to be similar to the (very small) differences discussed for the nonresonant spectra in Fig. 1. Instead, we attribute the (majority of the) shoulder to an ultrafast dissociation of the molecule on the time scale of the x-ray emission process. This interpretation is in accordance with resonant photoemission experiments of NH_3 in gas phase, where dissociation was observed when exciting into the $4a_1$ resonance.¹¹

A closer look at the participant emission gives further evidence for ultrafast dissociation and vibronic coupling in aqueous NH_3 and ND_3 . Three effects can be found for the participant emission: an increase of the intensity of the Rayleigh line close to the $4a_1$ and to the $2e$ absorption resonance (features C in Fig. 2), intensity on the low emission energy side of the Rayleigh line at the $4a_1$ and $2e$ absorption resonance (D in Fig. 2), and weak intensity in the region between participant and spectator emission at the $4a_1$ absorption resonance (E in Fig. 2). A close-up view of the $4a_1$ region is shown for aqueous NH_3 in Fig. 3(c) and aqueous ND_3 in Fig. 3(d). Note that in Fig. 3(c) the map information at excitation energies of 400.7 and 401.5 eV is distorted due to the formation of a gas bubble behind the SiC window membrane. The two intensity increases (C) of the Rayleigh line, one of which is visible in Figs. 3(c) and 3(d), can be explained by the presence of core-excitonic intermediate states with a large overlap between the one-electron wave function of the excited electron and the core hole, leading to an increased emission probability for elastic scattering.²⁶ Feature D results from vibronic coupling, as can be nicely derived from the vibrational signature for aqueous NH_3 , as indicated by the red arrows in Fig. 3(c). In Fig. 3(e), showing integrated spectra for excitation energies between 401.1 and 401.4 eV, a vibrational fine structure in the NH_3 spectrum is evident [for easier comparison, the spectra in Fig. 3(e) are shown on an energy scale relative to the peak maximum of the Rayleigh line and are normalized to the peak maximum]. Again, a significant isotope effect is observed, as will be discussed in the following.

The intensity distribution of the vibrational progression is governed by nuclear wave-packet (NWP) dynamics in the intermediate state, as was described by Hennies *et al.* for gas-phase oxygen and condensed-phase benzene and ethylene.^{12,27} The wave-packet dynamics are clearly visible in the difference between aqueous NH_3 and ND_3 in Figs. 3(c)–3(e) and are schematically illustrated in Fig. 4. At $t = 0$ (i.e., at the time of the absorption process), the nuclear wave function is identical to the wave function of the vibrational ground state in the electronic ground state [indicated by the blue Gaussians].

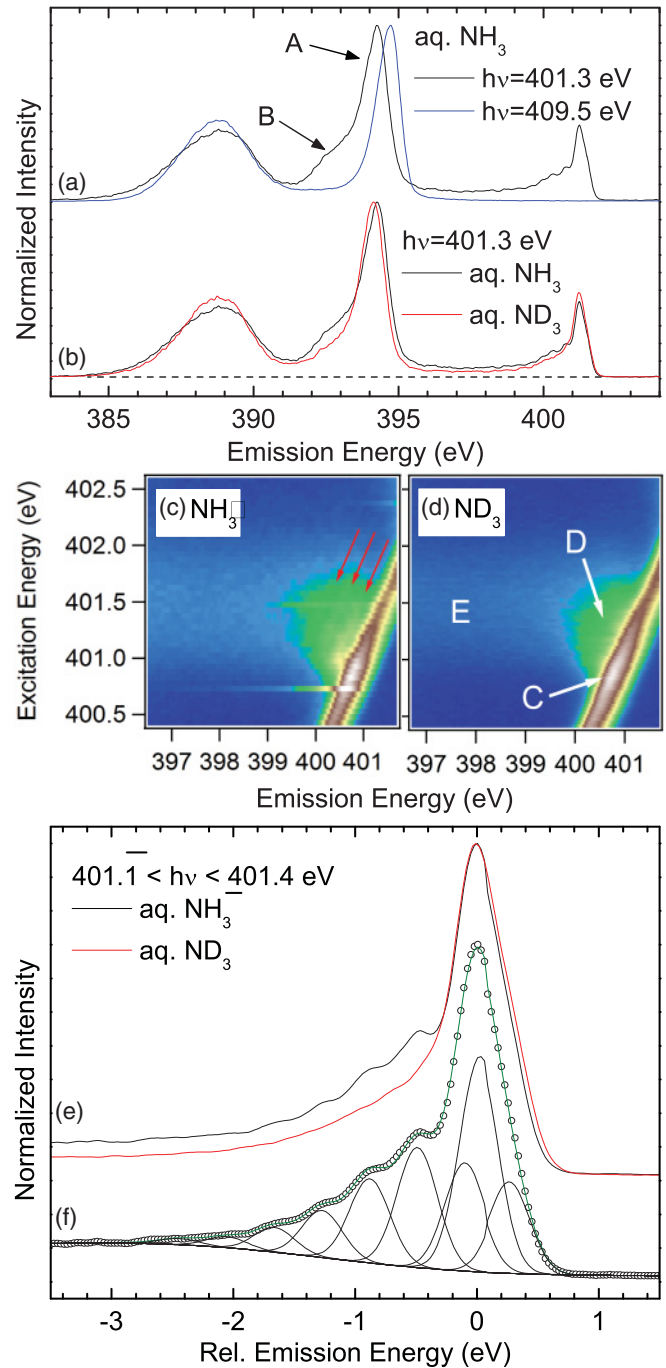


FIG. 3. (Color online) (a) NK emission spectra of aqueous NH_3 with nonresonant excitation (409.5 eV, blue) and excitation into the $4a_1$ resonance (401.3 eV, black). (b) NK emission spectra of aqueous NH_3 (black) and ND_3 (red) with excitation into the $4a_1$ resonance (401.3 eV). Detailed RIXS maps of (c) aqueous NH_3 (vibrational fine structure marked by red arrows) and (d) aqueous ND_3 . (e) Vibrational fine structure at the Rayleigh line of NH_3 (black) and ND_3 (red), integrated over excitation energies between 401.1 and 401.4 eV. (f) Data (circles) and fit (solid lines) of the vibrational fine structure of NH_3 .

During the duration of the x-ray emission process, the NWP develops (gray wave packets in Fig. 4), which happens faster for aqueous NH_3 than for ND_3 . While at $t = 0$ only emission to the vibrational ground state is possible (transition e in Fig. 4), more vibrational levels become accessible when the

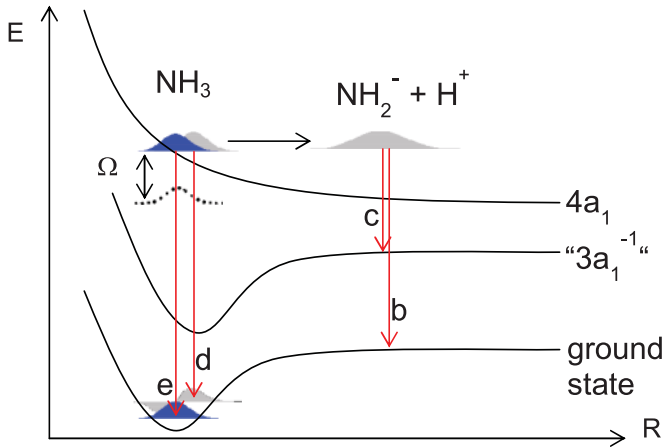


FIG. 4. (Color online) Schematic illustration of the wave-packet dynamics on the time scale of the x-ray emission process. The decay channels denoted with lower-case letters correspond to the decay-channel-specific absorption spectra shown in Fig. 5.

wave packet develops. As a result, higher vibrational levels are excited in NH_3 than in ND_3 (transitions d in Fig. 4). Thus, the vibrational progression is more pronounced and extends to lower emission energies for NH_3 than for ND_3 .

To derive an approximate value for the vibrational splitting of NH_3 , the spectrum in Fig. 3(e) was simulated using a fit with Gaussian functions, as shown in Fig. 3(f) (a correct description of the peak intensities within a consistent model is beyond the scope of this paper). Inspired by the analysis in Ref. 23 we suggest that each peak represents a sum over the lower energy vibrations of NH_3 . Seven equidistant Gaussians with identical width then represent the primary vibrational progression. Since a considerable amount of photons are elastically reflected at the window membrane, one additional Gaussian has to be used to account for this additional elastic scattering process. With this approach, we derive a vibrational splitting of (0.39 ± 0.05) eV. This value can be attributed to the symmetric stretching mode in the ground state of NH_3 ,²³ but is somewhat smaller than the gas-phase value of 0.414 eV.²⁴ While the difference is well within the error bar of our approach, this difference might hint towards the influence of the liquid environment on the potential energy surface of the NH_3 molecule.

A striking feature in the participant emission is the weak intensity in the region between Rayleigh line and spectator emission (E in Fig. 2), which is only present at the $4a_1$ resonance. We have previously observed such a broad loss distribution in the RIXS map of liquid H_2O and D_2O ,⁵ but could only speculate about its origin at that time. Here we propose that it results from the dissociation of the ammonia molecule at the $4a_1$ resonance. The final state of the (resonantly excited) dissociation consists of an NH_2^- (ND_2^-) radical and a proton (deuteron) with a certain kinetic energy, which gives rise to a homogeneous and broad energy-loss distribution (transitions b in Fig. 4). This interpretation is in agreement with the isotope effect, namely that [in Fig. 2 and Figs. 3(b) and 3(e)] feature E appears stronger for the faster-dissociating NH_3 than for ND_3 .

In the following, we will use the decay-channel-specific absorption spectra in Fig. 5, generated from the RIXS maps

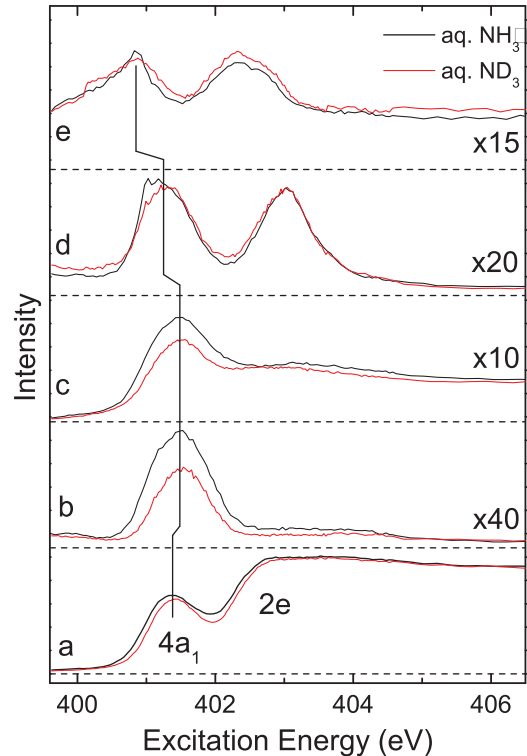


FIG. 5. (Color online) Decay-channel-specific absorption spectra of aqueous NH_3 (black) and aqueous ND_3 (red), integrated over the regions marked “a”–“e” in the ND_3 map in Fig. 2. For each spectrum, the magnification factors are given on the right. The vertical line indicates the position of the $4a_1$ resonance as a function of decay channel. The spectra correspond to the following decay channels: “a” all spectator decay channels, “b” dissociative decay channel, “c” dissociative decay channel in the spectator emission, “d” participant decay channel with vibrational coupling, “e” elastically scattered photons. Labels “b”–“e” correspond to the same labels in Fig. 4.

in Fig. 2, to give further evidence for our interpretation of molecular dissociation at the $4a_1$ resonance. The spectra in Fig. 5 were derived as follows: At each excitation energy, the emission intensity was integrated over suitably selected energy windows in between each pair of the white lines indicated in the RIXS map of aqueous ND_3 [Figs. 2(a)–2(e)], corresponding to Figs. 5(a)–5(e). For the two spectator decay windows “a” [broad window including all spectator emission, i.e., partial fluorescence yield (PFY)] and “c” (narrow window including feature B), the emission energy window was constant for all excitation energies. For the three participant decay windows “b” (region between participant and spectator decay), “d” (including features D), and “e” (Rayleigh line), the window was shifted parallel to the excitation energy (this corresponds to a constant energy window on an energy-loss scale). The widths of the energy windows were chosen such that they minimize contributions from neighboring features. The PFY spectra in Fig. 5(a) exhibit two main features, namely the $4a_1$ and $2e$ resonances, followed by flat and featureless curve progressions at higher excitation energies (note that, as is common with PFY spectra in the soft x-ray regime, saturation effects are expected to influence the intensity of spectral features, but not their line positions). Due to the different

vibrational structure, the $4a_1$ resonance has a smaller width for ND_3 than for NH_3 (as discussed earlier for the emission spectra as well). Compared to the PFY spectrum, all other decay-channel-specific absorption spectra exhibit energetic shifts of the $4a_1$ (and $2e$) resonance. To understand this behavior, it is important to consider the wave-packet dynamics illustrated in Fig. 4 together with the change of the duration time τ_{XES} of the x-ray emission process as a function of excitation energy. τ_{XES} is a function of the core-hole life time broadening Γ and the detuning energy Ω (see also Fig. 4): $\tau_{\text{XES}} = 1/\sqrt{\Omega^2 + \Gamma^2}$.²⁸ Thus, the more the excitation energy is detuned from the resonance, the shorter τ_{XES} and, consequently, the smaller the spectral contributions from processes involving dynamics in the excited state. At excitation energies below the $4a_1$ resonance, the x-ray emission process is too fast for the NWP to move, and thus vibrations are not excited nor does dissociation take place before emission. We then observe only the signature of the core exciton as an increase of the intensity of the Rayleigh line in Fig. 5(e). As the excitation energy is increased closer to the $4a_1$ resonance, the detuning energy Ω decreases and τ_{XES} increases, which, at some point, allows enough time for the NWP to excite vibrations [Fig. 5(d)]. This reduces the intensity of the Rayleigh line [Fig. 5(e)] and, ultimately, allows the nuclear NWP to move far enough to dissociate the molecule [Figs. 5(b) and 5(c)]. A similar behavior is found at the $2e$ absorption resonance, namely enhanced intensity of the Rayleigh line below the $2e$ resonance [Fig. 5(e)] and the onset of vibrations at the $2e$ resonance [Fig. 5(d)]. In contrast, however, we find that the emission channels indicative for dissociation [Figs. 5(b) and 5(c)] do *not* show a resonance [note that the remaining intensity in Fig. 5(c) above an excitation energy of ~ 402 eV can be attributed to the tail of the $3a_1^{-1}$ emission, which is included in the integrated emission energy window]. The presence (absence) of the resonance in the “dissociation channels” allows us to directly identify the $4a_1$ resonance as being dissociative, while no dissociation occurs at the $2e$ resonance.

Having thus established the dissociation behavior of aqueous ammonia upon resonant excitation, we go back to the

emission spectra in Fig. 3 and use the relative intensities of the spectral features A and B in the spectator decay to estimate a dissociation time τ_D for the $4a_1$ core-excited state. The intensities of features A and B were determined by fitting the $2a_1^{-1}$ emission lines of Fig. 3(b) with two components, one with the nonresonant $2a_1^{-1}$ line shape (feature A) and one with a Gaussian line shape (feature B). Following the approach in Ref. 13 we can use the intensities of features A I_A and B I_B and the N $1s$ core-hole lifetime broadening Γ of ~ 110 meV²⁹ to derive τ_D :¹³ $\tau_D = -\hbar/2\Gamma \cdot \ln(1 - I_B/I_A)$. With this we estimate τ_D to be 9 ± 2 fs for aqueous NH_3 and 12 ± 2 fs for aqueous ND_3 (error bars are solely based on the uncertainty in the intensity ratio of features A and B). These times are much shorter than the ones derived in Ref. 11 for gas phase NH_3 (32 fs), which suggests that the hydrogen-bonding environment in the solution accelerates the dissociation process significantly.

IV. CONCLUSIONS

In summary, we have investigated the nuclear dynamics in the core-excited state of aqueous NH_3 and ND_3 using resonant inelastic soft x-ray scattering. We find strong vibronic coupling in the $4a_1$ and $2e$ excited states and achieve vibrational resolution for aqueous NH_3 . The observed strong isotope effect for aqueous NH_3 and ND_3 gives clear evidence for ultrafast dissociation on the time scale of the x-ray emission process when exciting into the $4a_1$ resonance, while the $2e$ resonance is identified as nondissociative on the time scale of the x-ray emission process.

ACKNOWLEDGMENTS

This work was supported by the German BMBF (Project Nos. 05KS4WWA/6 and 05KS4VHA/4). M. Bär acknowledges the financial support by the Impuls- und Vernetzungsfonds of the Helmholtz Association (Contract No. VH-NG-423). The ALS is supported by the Department of Energy, Basic Energy Sciences, Contract No. DE-AC02-05CH11231.

*Corresponding author: lothar.weinhardt@physik.uni-wuerzburg.de

[†]MPI for Intelligent Systems, Heisenbergstrasse 3, D-70569 Stuttgart, Germany.

¹S. Myneni, Y. Luo, L.-A. Naslund, M. Cavalleri, L. Ojamäe, H. Ogasawara, A. Pelmenschikov, Ph. Wernet, P. Väterlein, C. Heske, Z. Hussain, L. G. M. Pettersson, and A. Nilsson, *J. Phys. Condens. Matter* **14**, L213 (2002).

²J. D. Smith, C. D. Cappa, K. R. Wilson, B. M. Messer, R. C. Cohen, and R. J. Saykally, *Science* **306**, 851 (2004).

³Ph. Wernet, D. Nordlund, U. Bergmann, M. Cavalleri, M. Odelius, H. Ogasawara, L.-Å. Näslund, T. K. Hirsch, L. Ojamäe, P. Glatzel, L. G. M. Pettersson, and A. Nilsson, *Science* **304**, 995 (2004).

⁴J.-H. Guo, Y. Luo, A. Augustsson, S. Kashtanov, J.-E. Rubensson, D. K. Shuh, H. Ågren, and J. Nordgren, *Phys. Rev. Lett.* **91**, 157401 (2003).

⁵L. Weinhardt, O. Fuchs, M. Blum, M. Bär, M. Weigand, J. D. Denlinger, Y. Zubavichus, M. Zharnikov, M. Grunze, C. Heske,

and E. Umbach, *J. Electron Spectrosc. Relat. Phenom.* **177**, 206 (2010).

⁶O. Fuchs, M. Zharnikov, L. Weinhardt, M. Blum, M. Weigand, Y. Zubavichus, M. Bär, F. Maier, J. D. Denlinger, C. Heske, M. Grunze, and E. Umbach, *Phys. Rev. Lett.* **100**, 027801 (2008).

⁷M. Odelius, *Phys. Rev. B* **79**, 144204 (2009).

⁸T. Tokushima, Y. Harada, O. Takahashi, Y. Senba, H. Ohashi, L. G. M. Pettersson, A. Nilsson, and S. Shin, *Chem. Phys. Lett.* **460**, 387 (2008).

⁹T. Tokushima, Y. Harada, Y. Horikawa, O. Takahashi, Y. Senba, H. Ohashi, L. G. M. Pettersson, A. Nilsson, and S. Shin, *J. Electron Spectrosc. Relat. Phenom.* **177**, 192 (2010).

¹⁰O. Fuchs, M. Zharnikov, L. Weinhardt, M. Blum, M. Weigand, Y. Zubavichus, M. Bär, F. Maier, J. D. Denlinger, C. Heske, M. Grunze, and E. Umbach, *Phys. Rev. Lett.* **100**, 249802 (2008).

¹¹I. Hjelte, M. N. Piancastelli, C. M. Jansson, K. Wiesner, O. Björneholm, M. Bässler, S. L. Sorensen, and S. Svensson, *Chem. Phys. Lett.* **370**, 781 (2003).

- ¹²F. Hennies, A. Pietzsch, M. Berglund, A. Föhlisch, Th. Schmitt, V. Strocov, H. O. Karlsson, J. Andersson, and J.-E. Rubensson, *Phys. Rev. Lett.* **104**, 193002 (2010).
- ¹³A. Naves de Brito, A. Naves de Brito, O. Björneholm, J. S. Neto, A. B. Machado, S. Svensson, A. Ausmees, S. J. Osborne, L. J. Sæthre, H. Aksela, O.-P. Sairanen, A. Kivimäki, E. Nömmiste, and S. Aksela, *J. Mol. Struct.: Theochem* **394**, 135 (1997).
- ¹⁴O. Björneholm, S. Sundin, S. Svensson, R. R. T. Marinho, A. Naves de Brito, F. Gel'mukhanov, and H. Ågren, *Phys. Rev. Lett.* **79**, 3150 (1997).
- ¹⁵S. Sundin, F. Kh. Gel'mukhanov, H. Ågren, S. J. Osborne, A. Kikas, O. Björneholm, A. Ausmees, and S. Svensson, *Phys. Rev. Lett.* **79**, 1451 (1997).
- ¹⁶F. Hennies, S. Polyutov, I. Minkov, A. Pietzsch, M. Nagasono, F. Gel'mukhanov, L. Triguero, M.-N. Piancastelli, W. Wurth, H. Ågren, and A. Föhlisch, *Phys. Rev. Lett.* **95**, 163002 (2005).
- ¹⁷M. Odelius, H. Ogasawara, D. Nordlund, O. Fuchs, L. Weinhardt, F. Maier, E. Umbach, C. Heske, Y. Zubavichus, M. Grunze, J. D. Denlinger, L. G. M. Pettersson, and A. Nilsson, *Phys. Rev. Lett.* **94**, 227401 (2005).
- ¹⁸L. Weinhardt, O. Fuchs, A. Fleszar, M. Bär, M. Blum, M. Weigand, J. D. Denlinger, W. Yang, W. Hanke, E. Umbach, and C. Heske, *Phys. Rev. B* **79**, 165305 (2009).
- ¹⁹J. Schirmer, A. B. Trofimov, K. J. Randall, J. Feldhaus, A. M. Bradshaw, Y. Ma, C. T. Chen, and F. Sette, *Phys. Rev. A* **47**, 1136 (1993).
- ²⁰J. Nordgren, H. Agren, L. O. Werme, C. Nordling, and K. Siegbahn, *J. Phys. B: At. Mol. Phys.* **9**, 295 (1976).
- ²¹O. Fuchs, L. Weinhardt, M. Blum, M. Weigand, E. Umbach, M. Bär, C. Heske, J. Denlinger, Y. D. Chuang, W. McKinney, Z. Hussain, E. Gullikson, M. Jones, P. Batson, B. Nelles, and R. Follath, *Rev. Sci. Instrum.* **80**, 63103 (2009).
- ²²M. Blum, L. Weinhardt, O. Fuchs, M. Bär, Y. Zhang, M. Weigand, S. Krause, S. Pookpanratana, T. Hofmann, W. Yang, J. D. Denlinger, E. Umbach, and C. Heske, *Rev. Sci. Instrum.* **80**, 123102 (2009).
- ²³H. Ågren, J. Müller, and J. Nordgren, *J. Chem. Phys.* **72**, 4078 (1980).
- ²⁴T. Shimanouchi, Natl. Stand. Ref. Data Ser. (US, Natl. Bur. Stand.) **39**, 1 (1972).
- ²⁵F. Gel'mukhanov and H. Ågren, *Phys. Rev. A* **54**, 3960 (1996).
- ²⁶L. Weinhardt, O. Fuchs, D. R. Batchelor, M. Bär, M. Blum, J. D. Denlinger, W. Yang, A. Schöll, F. Reinert, E. Umbach, and C. Heske, *J. Chem. Phys.* (in print, 2011).
- ²⁷F. Hennies, S. Polyutov, I. Minkov, A. Pietzsch, M. Nagasono, H. Ågren, L. Triguero, M.-N. Piancastelli, W. Wurth, F. Gel'mukhanov, and A. Föhlisch, *Phys. Rev. A* **76**, 032505 (2007).
- ²⁸F. Gel'mukhanov and H. Ågren, *Phys. Rep.* **312**, 87 (1999).
- ²⁹K. C. Prince, M. Vondráček, J. Karvonen, M. Coreno, R. Camilloni, L. Avaldi, and M. de Simone, *J. Electron Spectrosc. Relat. Phenom.* **101-103**, 141 (1999).